Analyst

ROYAL SOCIETY
OF **CHEMISTRY** | Celebrating
IYPT 2019

PAPER
Jaebum Choo, Fabiao Yu *et al.*
SERS-based immunoassay using gold-patterned array chips
for rapid and sensitive detection of dual cardiac biomarkers

SERS-based immunoassay using gold-patterned array chips for rapid and sensitive detection of dual cardiac biomarkers†

Ziyi Cheng,‡[a] Rui Wang,‡[a] Yanlong Xing,[a] Linlu Zhao,[a] Jaebum Choo [ID] *[b] and Fabiao Yu [ID] *[a]

Cardiac troponin I (cTnI) and creatine kinase-MB (CK-MB) are important diagnostic biomarkers for acute myocardial infarction (AMI). Many efforts have been undertaken to develop highly sensitive detection methods for the quantitative analysis of these dual targets. However, current immunoassay methods are inadequate for accurate measurement of cTnI and CK-MB, due to their limited detection sensitivity. Thus, there is still an urgent demand for a new technique that will enable ultrahigh sensitive detection of these biomarkers. In this study, we developed a surface-enhanced Raman scattering (SERS)-based sandwich immunoassay platform for the ultrasensitive detection of cTnI and CK-MB. In this study, a monoclonal-antibody-immobilized gold-patterned chip was used as a SERS active template. Target samples and poly-clonal-antibody-conjugated Au@Ag core−shell nanoparticles were then added. Using this SERS platform, the concentration of biomarkers could be quantified by monitoring the characteristic Raman peak intensity of Raman reporter molecules. Under optimized conditions, the limits of detection (LODs) were estimated to be 8.9 pg mL^{-1} and 9.7 pg mL^{-1} for cTnI and CK-MB, respectively. Thus, the proposed SERS-based immunoassay has great potential to be an effective diagnostic tool for the rapid and accurate detection of cTnI and CK-MB.

Introduction

Acute myocardial infarction (AMI), a severe cardiovascular disease, is one of the leading causes of death in developed and developing countries.[1] As a result, the need for rapid and accurate diagnosis of AMI has gained increasing attention from many researchers.[2,3] Therefore, a sensitive and cost-efficient assay is in demand in order to fulfill the diagnostic requirements of AMI.[4–6] Cardiac biomarkers play vital roles in the diagnosis, prognosis, and risk stratification of heart-attack patients.[7] The ideal selection of AMI biomarkers should obey the following principles: (1) sufficient concentration in the myocardium; (2) negligible concentration in noncardiac tissues; (3) high sensitivity and specificity toward AMI. Several biomarkers have been employed in the past, including lactate dehydrogenase isoenzymes, myoglobin (Mb), and aspartate aminotransferase, but they proved unsatisfactory due to their low specificity.[8] Instead, cardiac troponin I (cTnI), creatine kinase-MB (CK-MB),[9] and cardiac forms of troponin T (cTnT)[10] have become more popular diagnostic biomarkers for AMI in *in vitro* diagnostics. Among them, cTnI has been regarded as a current "gold standard" for the diagnosis of AMI, due to its high specificity and sensitivity.[11] It takes approximately 4 h for cTnI to reach detectable concentrations after the onset of AMI, and cTnI levels remain elevated for 4–10 d after onset. This indicates that its concentration remains elevated for long enough to allow a suitable diagnostic window. By contrast, CK-MB appears 5–6 h after the onset of AMI and remains abnormally elevated for 12–24 h. Therefore, the measurement of these two biomarkers is effective in AMI diagnosis and is also useful in monitoring reinfarction.[12] According to clinical reports,[13] the clinical cutoff levels are 0.06–1.5 ng mL^{-1} and 3.5–10 ng mL^{-1} for cTnI and CK-MB, respectively. Because the biomarkers have different characteristics and their release time scales after symptom onset differ, simultaneous detection of cTnI and CK-MB can overcome the drawbacks of single biomarker detection and increase the probability of early diagnosis of AMI.[14]

Many efforts have been made to develop highly sensitive detection methods for cTnI and CK-MB using enzyme-linked

[a]Institute of Functional Materials and Molecular Imaging, Key Laboratory of Emergency and Trauma, Ministry of Education, Key Laboratory of Hainan Trauma and Disaster Rescue, College of Clinical Medicine, College of Emergency and Trauma, Hainan Medical University, Haikou 571199, China. E-mail: fbyu@yic.ac.cn
[b]Department of Chemistry, Chung-Ang University, Seoul 06974, South Korea. E-mail: jbchoo@cau.ac.kr
†Electronic supplementary information (ESI) available. See DOI: 10.1039/c9an01260e
‡Co-first author.

immunosorbent assays (ELISA),[15,16] fluorescence,[17,18] electrochemistry[19,20] and surface plasmon resonance (SPR).[21,22] ELISA is based on the principle that light of a specific wavelength will be absorbed by a chromogenic reaction in the presence of analytes. Although ELISA has been widely used to screen for cTnI and CK-MB and many ELISA kits have been commercialized for this purpose, this approach has several drawbacks, including long incubation time, multiple washing steps, and low sensitivity. Therefore, this method does not meet the requirements for rapid and highly sensitive assessment of cTnI and CK-MB. Fluorescence immunoassay addresses the sensitivity issue, but photobleaching interferes with the stable detection of target biomarkers. The electrochemical method, by contrast, also has problems of sensitivity, and is susceptible to noise. Therefore, there is still an urgent need for the development of a sensitive detection technique of cTnI and CK-MB in routine clinical diagnosis.

Recently, surface-enhanced Raman scattering (SERS)-based immunoassay has garnered increasing attention due to its high sensitivity and potential for multiplex detection capability.[23,24] Many different types of biomarkers, including proteins, small molecules, and pathogens, have been successfully investigated through SERS-based immunoassay techniques.[25] In a SERS-based immunoassay, Raman scattering signals of reporter molecules can be significantly enhanced at the SERS active sites, known as "hot spots", using electromagnetic and chemical enhancements.[26] This can be used to overcome the low sensitivity inherent in conventional Raman spectroscopy. To date, many different types of SERS probes based on different metal nanostructures, including nanospheres, core-shells, hollows, and nanoclusters, have been proposed for this purpose.[27–30] These probes interactions with SERS-active substrates play essential roles in detection sensitivity, allowing "hot spots" to emerge at junctions between the probes and substrates when the two are placed in a sandwich format. This discovery opens opportunities to employ SERS-active substrates, combined with SERS nanoprobes, for ultrasensitive detection.

In this study, a gold-patterned chip has been used for the SERS-based immunoassay of the biomarkers cTnI and CK-MB, together with Au@Ag core–shell nanoparticles. To capture target antigens, monoclonal antibodies of these two biomarkers have been immobilized on the surface of a gold-patterned chip. Next, polyclonal-antibody-conjugated Au@Ag core–shell SERS probes have been added to form sandwich immunocomplexes. Quantitative analysis of these biomarkers can then be performed by monitoring the characteristic Raman peak intensity of Raman reporter molecules immobilized on SERS probes. We believe that the proposed SERS-based assay protocol using a gold patterned array chip and core–shell nanoparticles opens a new opportunity for the early diagnosis of AMI.

Experimental section

Materials

Gold(III) chloride trihydrate (HAuCl$_4$·3H$_2$O), thiols-poly (ethylene glycol)-COOH (HS-PEG-COOH, MW ~ 7500), 11-mercapto-undecanoic acid (11-MUA), and poly (ethylene glycol) methyl ether thiol (HS-PEG, MW ~ 1500) were purchased from Sigma-Aldrich (St Louis, MO, USA). Malachite green isothiocyanate (MGITC) was purchased from Invitrogen (Carlsbad, CA, USA). Mouse anti-cTnI monoclonal antibody (ab10231), rabbit anti-cTnI polyclonal antibody (ab47003), mouse anti-CK-MB monoclonal antibody (ab404) and rabbit anti-CK-MB polyclonal antibody (ab31832) were purchased from Abcam (Shanghai, China). Silver nitrate, 3-aminopropyltrimethoxysilane (APTES) and phosphate-buffered saline (PBS) were purchased from Aladdin (Shanghai, China). The ultrapure water (18 MΩ cm^{-1}) used in this study was prepared by a Milli-Q water purification system (Billerica, MA, USA). All the other reagents were from commercial sources with analytical reagent grade and used without any further purification.

Instruments

Raman measurements were obtained using a Renishaw inVia Raman microscope system (Renishaw, New Mills, UK) equipped with a high-resolution grating with 1800 grooves per cm. Spectra were acquired using a 632.8 nm excitation laser with a power of 17 mW. The Rayleigh line was removed from the collected Raman scattering using a holographic notch filter located in the collection path. Wavelength calibration was performed by measuring a silicon wafer and evaluating the first-order phonon band of 520 cm^{-1}. The baselines of all Raman spectra were corrected to remove background noises using the WiRE software suite (Renishaw, New Mills, UK). A CCD camera was fitted to an optical microscope to obtain optical images. A 20× objective lens was used to focus a laser spot on the gold chip. All Raman spectra reported in this study were collected using 1 s exposure time and 1 accumulation in the range of 630–1730 cm^{-1}. The UV-vis absorption spectra were obtained on a UV-1800 spectrophotometer (Shimadzu, Japan). Dynamic light scattering (DLS) data were collected from a Nano-ZS90 particle size analyzer (Malvern, UK). Transmission electron microscopy (TEM) images were gained using a JEOL JEM 2100F (Japan) instrument at an accelerating voltage of 200 kV.

Preparation of SERS probes

Gold nanoparticles were prepared using the previously reported seed-growth method with minor modification.[31] All glassware was washed in aqua regia and then rinsed with ultrapure water and oven-dried before use. A 2.2 mM sodium citrate solution was heated to boiling. Next, 0.5 mL of 25 mM HAuCl$_4$ was added to the solution, which was then vigorously stirred and boiled. The color changed from light yellow to bluish grey, and then to soft pink, in 15 min. The resulting gold seed solution was then cooled to 90 °C. After this, 0.5 mL of 60 mM sodium citrate and 0.5 mL of 25 mM HAuCl$_4$ solution were added. This was repeated 12 times at 2 min intervals, to ensure complete mixing after each addition. Eventually, the color of the solution changed from pink to deep red. The solution was stirred for an additional 30 min at 90 °C and then cooled to room temperature. The shape and size distribution

of gold nanoparticles (AuNPs) was characterized by DLS and TEM.

Au@Ag core–shell nanoparticles were synthesized through the reduction of silver nitrate by ascorbic acid. Briefly, 10 mM of ascorbic acid was added into 5 mL of AuNPs under vigorous stirring. Then, 10 mM of silver nitrate was dropped into the mixture and reacted for 1 h. The silver thickness was controlled by changing the volume of the silver staining solution. The optimal silver shell thickness was estimated to be 4 nm. The characteristics of Au@Ag core–shell nanoparticles were investigated using UV-vis, DLS, TEM, and SERS measurements.

SERS probes were prepared after the synthesis of Au@Ag nanoparticles. MGITC solution in isopropanol (0.5 μL, 10^{-2} M) was added to 1.0 mL of AuNPs (~40 nm). After 30 min the solution of 10 mM ascorbic acid was mixed with the MGITC-labeled AuNPs, and 10 mM of silver nitrate was dropped under stirring. The mixture stirred for 1 h. Then, 0.5 μL of MGITC (10^{-2} M) was added to the Au@Ag nanoparticles and reacted for 30 min. Antibody conjugation was carried out through the activated heterofunctional linker HS-PEG-COOH. The HS-PEG-COOH (60 μL, 10 μM) was dropped into 1.0 mL of MGITC-labeled Au@Ag nanoparticles under vigorous stirring, creating a solution of PEGlyated nanoparticles. After 30 min of continuous stirring, the HS-PEG solution (120 μL, 10 μM) was added into the PEGlyated Au@Ag nanoparticles and reacted for 3 h. Subsequently, the PEGlyated Au@Ag nanoparticles were centrifuged (7000 rpm, 10 min) to remove unbound PEG molecules and then resuspended in PBS (pH 7.2, 50 mM).

To activate the –COOH groups that conjugated to the surface of Au@Ag nanoparticles, 1-ethyl-3-(3-dimethyl-aminopropyl) carbodiimide (EDC) (10 μL, 25 mM) and N-hydroxysulfosuccinimide (NHS) (10 μL, 25 mM) were mixed vigorously at 25 °C for 15 min. Excess EDC and NHS were separated from the activated Au@Ag nanoparticles through centrifugation (7000 rpm, 10 min, 3 rounds), and re-dispersed in a PBS buffer solution (pH 7.2, 50 mM). Then, mouse anti-cTnI monoclonal antibody (ab10231) and mouse anti-CK-MB monoclonal antibody (ab404) were added into the MGITC-labeled Au@Ag core–shell nanoparticles with activated carboxyl groups and reacted for 2 h, respectively. The reaction mixture was then stored at 4 °C overnight. Excess antibodies were removed through centrifugation (7000 rpm, 10 min, 3 rounds) and resuspended in a PBS (50 mM, pH 7.4) buffer.

Fabrication of gold-patterned chip

Home-made AuNPs were deposited on the surface of silicon wafers by the immersion method. Initially, silicon wafers were treated with piranha solution (1 : 1 in a volume of $H_2SO_4 : H_2O_2$) for 30 min to expose –OH groups on the surface, then washed with deionized water and subsequently dried with nitrogen gas. The substrate was then immersed in a 10% ethanol solution of APTES to link –OH groups on the surface. Next, AuNPs adsorption was induced by immersion of the substrate in the aqueous solution with gold nanoparticles. The amino terminal groups displaced the citrate groups to chemi-

cally fix AuNPs to the surface. Finally, the functionalized silicon wafers were assembled on the glass slide to obtain a gold-patterned chip.

Results and discussion

Protocols of SERS-based immunoassay

Scheme 1 illustrates the procedure of SERS-based immunoassay for the quantification of cTnI and CK-MB. Firstly, the surface of the chip was modified with carboxyl groups through the addition of 11-MUA. To activate the carboxyl group-modified gold chip, 5 μL of 25 mM EDC and 5 μL of 25 mM NHS were dropped on each chip section and then incubated for 30 min. The non-reacted EDC/NHS was removed by washing with a phosphate buffer solution containing 0.02% Tween 20 (PBST) and then dried with nitrogen gas. Afterward, 3 μL of 100 μg mL^{-1} rabbit anti-cTnI polyclonal antibody (ab47003) and rabbit anti-CK-MB polyclonal antibody (ab31832) in PBS were dropped onto different sections of the NHS-activated chip and incubated for 1 h, respectively. The unbound antibodies were removed through washing three times with PBST. Next, 3 μL of different concentrations of cTnI and CK-MB antigens (0, 0.01, 0.1, 1, 10, 20, 50 and 100 ng mL^{-1}) in PBS buffer containing 1% BSA (weight ratio) were dropped onto each well and incubated for 1 h. Then, the chip was washed with PBST three times and dried with nitrogen gas. Finally, 3 μL of cTnI and CK-MB SERS probes were introduced onto the wells. The mixture was reacted for 1 h to form sandwich immunocomplexes before the SERS detection. Herein, MGITC was used as a Raman reporter molecule due to its intense SERS signal. The Raman peak centered at 1615 cm^{-1}, which shows the strongest peak intensity, was used for the quantitative evaluation of cTnI and CK-MB.

Optimization of SERS-active Au@Ag core–shell nanoparticles

Many different types of SERS nanoprobes have been developed for sensitive and reproducible signal enhancement. In the present study, Au@Ag core–shell nanoparticles, including MGITCs as Raman reporter molecules, were used as SERS nanoprobes (Fig. 1). MGITC molecules were attached on the surface of 40 nm gold nanoparticles, and then silver nitrate was reduced by ascorbic acid to form a silver shell around the nanoparticles. Additionally, a second layer of MGITC was formed on the surface of the silver shell to further enhance the Raman signal intensity (Fig. 1A). TEM imagery and DLS data of the gold nanoparticles used in this study are displayed in Fig. S1.† The silver shell thickness was controlled by changing the volume of the silver-staining solution applied during preparation. As shown in the TEM images (Fig. S2†), the thickness of the silver shell was proportional to the volume of silver staining solution. The red color of AuNPs gradually changed to yellow with the increase of shell thickness (Fig. 1B). The shell thickness grew from 2 to 5 nm as the volume of silver staining solution was increased from 20 μL to 80 μL, as shown in Fig. 1C. As shown in Fig. 1D, the UV-vis spectrum also illus-
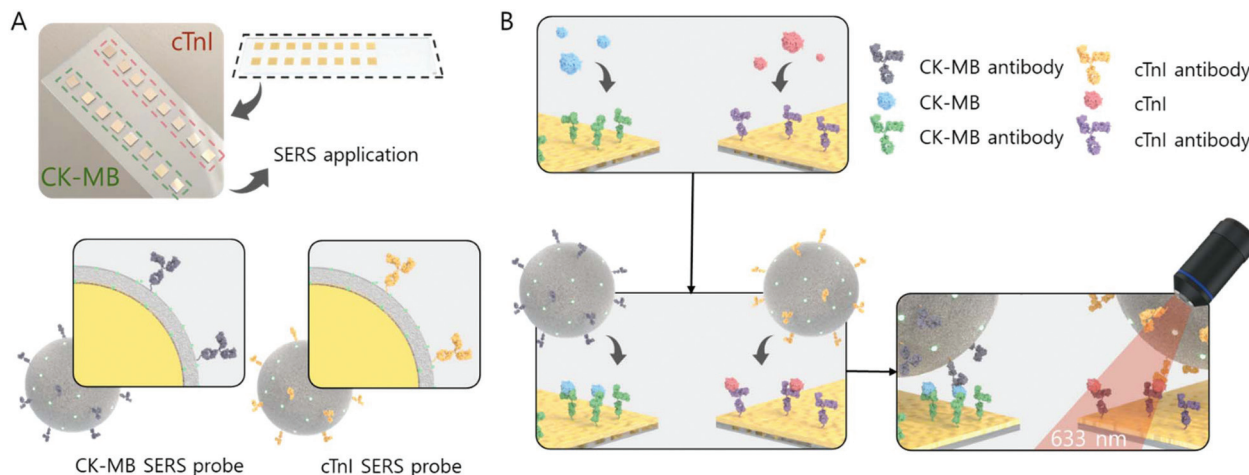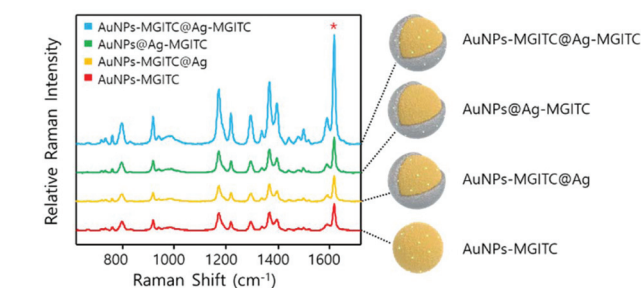
Scheme 1 Schematic illustration of SERS-based sandwich immunoassays for quantitative analysis of cTnI and CK-MB. (A) Gold-patterned chip and SERS probes for the detection of dual biomarkers. (B) Monoclonal antibodies conjugated (cTnI and CK-MB) onto the gold-patterned chip for the capture of target antigens. SERS probe addition for the formation of sandwich immunocomplexes. Raman detection of immunocomplexes using 632.8 nm laser.
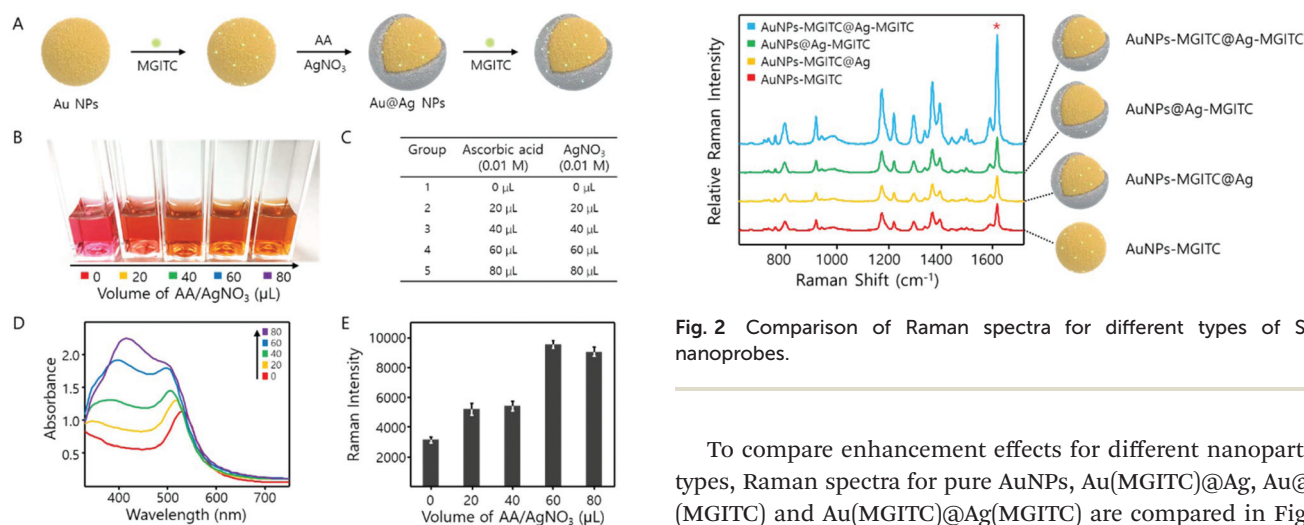
Fig. 1 Fabrication and characterization of Au@Ag core−shell nanoparticles. (A) Fabrication process of MGITC-labeled Au@Ag core−shell nanoparticles. (B) Photographic images for different thickness of Ag shell. (C) Different volumes of AA and AgNO₃ silver-staining solutions for the control of silver thickness. (D) Corresponding UV-vis spectra. (E) Variation of SERS signal intensity at 1615 cm⁻¹ for different silver staining solutions.
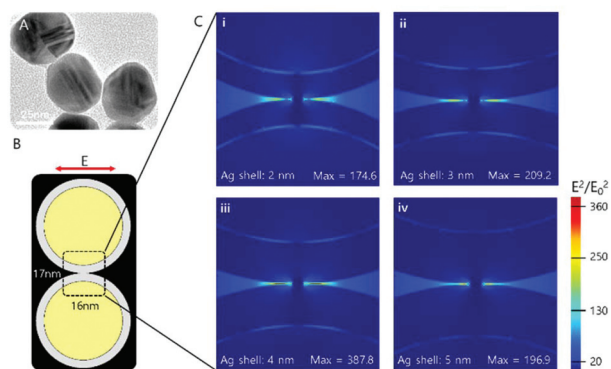

Fig. 2 Comparison of Raman spectra for different types of SERS nanoprobes.

To compare enhancement effects for different nanoparticle types, Raman spectra for pure AuNPs, Au(MGITC)@Ag, Au@Ag (MGITC) and Au(MGITC)@Ag(MGITC) are compared in Fig. 2. As expected, Au(MGITC)@Ag(MGITC) shows much stronger Raman signal intensity at 1615 cm⁻¹ than the other types of nanoparticles under the same detection conditions. This is because the double-layer immobilizes more Raman reporter molecules on the surface of the gold core and silver shell. As a result, its Raman spectrum shows a stronger SERS signal intensity than other structures.

FDTD simulation of Au@Ag nanoparticles with different thickness of silver shell

To better understand the SERS enhancement effects as a function of the silver shell thickness, finite-difference-time-domain (FDTD) calculations were performed to examine the distribution of local electric field strength for different shell thicknesses (Fig. 3). In this experiment, a gold-patterned chip was used as a substrate to capture SERS probes, and it was expected that the gap between Au@Ag core−shell nanoparticles

trates that the characteristic surface plasmon band of silver at 420 nm increased with the shell thickness. It was found that the SERS signal intensity at 1615 cm⁻¹ was also gradually increased with silver shell thickness, up to a thickness of 4 nm, but decreased when the thickness reached 5 nm (Fig. 1E). Therefore, the optimum silver shell thickness was estimated to be 4 nm, and Au@Ag nanoparticles with 4 nm of thickness shell were used for further experiments.
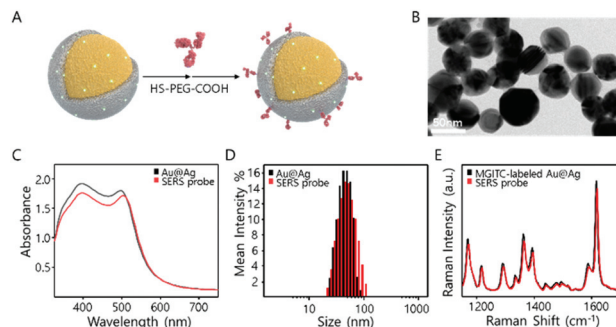
Fig. 3 (A) TEM image of Au@Ag core–shell nanoparticles. (B) Two-dimensional model of two Au@Ag core–shell nanoparticles in FDTD simulation. The red arrow indicates the polarization direction of the incident light. (C) Maps for the enhancement of local electric fields under the illumination of a linearly polarized wave. Computational simulations were performed for Au@Ag nanoparticles with four different thicknesses of sliver shell (i: 2 nm, ii: 3 nm, iii: 4 nm and iv: 5 nm). The scale bar shows a colour decoding bar for different Raman intensities.

Fig. 4 Preparation and characterization of antibody-conjugated Au@Ag core–shell SERS nanoprobes. (A) Antibody conjugation on the surface of nanoparticles. (B) TEM image of SERS nanoprobes. (C) DLS distributions, (D) UV-vis spectra and (E) SERS spectra of nanoparticles before (black) and after (red) bioconjugation.

and the chip surface partially contributes to the electromagnetic enhancement. However, it was previously reported that the enhancement effects from the "hot spots" at the nanoparticle-to-nanoparticle junction sites are still dominant.[32] Fig. 3A shows the TEM image of aggregated nanoparticles on a gold-patterned substrate.

To further investigate these phenomena, FDTD simulations for the "hot spots" between two Au@Ag core–shell particles were performed. Herein, a two-dimensional simulation model of two nanoparticles was set up (Fig. 3B), and the wavelength of incident light in FDTD simulations was set to 632.8 nm. The scale bar at the right side of the figure displays the color decoding for different Raman intensities. Based on the FDTD simulations, the E^2/E_0^2 distributions of transverse plasmon excitations between two particles along the silver shell thickness are displayed in Fig. 3C(i–iv). As shown in this figure, the E^2/E_0^2 distributions show the strongest electromagnetic field enhancement when the silver thickness is 4 nm in Fig. 3C(iii). This intensity is approximately 2.2 times stronger than that of 2 nm Ag shell thickness. This result coincides with the previous experimental results. FDTD simulations suggest that the 4 nm Ag shell thickness provides a maximum EM enhancement and it also explains the strong Raman intensity of 4 nm Ag coated Au nanoparticles in Fig. 1E.

Antibody conjugations on the surface of Au@Ag core–shell nanoparticles and fabrication process of gold-patterned array chip

Rabbit polyclonal cTnI antibodies were conjugated on the surface of Au@Au core–shell nanoparticles, as illustrated in Fig. 4A. The TEM image in Fig. 4B shows that the particles keep the sphere morphologies. The DLS data in Fig. 4C demonstrate that the average diameter is slightly increased after bioconjugation. From UV-vis (Fig. 4D) and SERS (Fig. 4E)

spectra, no conspicuous changes were observed before and after the bioconjugation, indicating the bioconjugation did not significantly affect their SERS activities.

As shown in Fig. 5A, a bio-functionalized gold-patterned array chip was prepared by four-step processes, as described in the Experimental section. To investigate the reproducibility of the gold-patterned array chip, 0.01 mM MGITC was labeled on the surface of the chip and Raman spectra were recorded for 9 randomly selected spots. Corresponding Raman spectra revealed no significant variations among different detection points, as shown in Fig. 5B, thus demonstrating prominent repeatability of the designed gold-patterned array chip.

Reproducibility and repeatability tests of SERS-based assay

To evaluate the reproducibility and repeatability of the SERS-based assay for cTnI and CK-MB, recovery tests for normal human serum samples spiked with cTnI and CK-MB were also performed. As shown in Table 1, the recovery percentages of cTnI and CK-MB spiked serum samples range from 97.3% to 113.2%, which indicated a good reproducibility of proposed SERS-based assay technique. The average coefficient of variance (CV, %) value between biological replicates is below 16%. The recovery (%) and CV (%) are listed in Table 1.

Selectivity test

To test the specificity of the SERS-based immunoassay for cTnI and CK-MB, we performed selectivity tests for several non-specific proteins including human immunoglobulin G (IgG), human serum albumin (HSA), bovine serum albumin (BSA), myoglobin (MYO) and creatine kinase (CK) as shown in Fig. S3.† As expected, only cTnI and CK-MB could induce the great increase of SERS signal, while no obvious changes in intensity were observed for other proteins. This observation indicates that the interaction between antibodies and a target antigen is significantly stronger than that of other non-specific antigens. All the results illustrated that this proposed SERS-based immunoassay possessed excellent specificity toward target antigens.
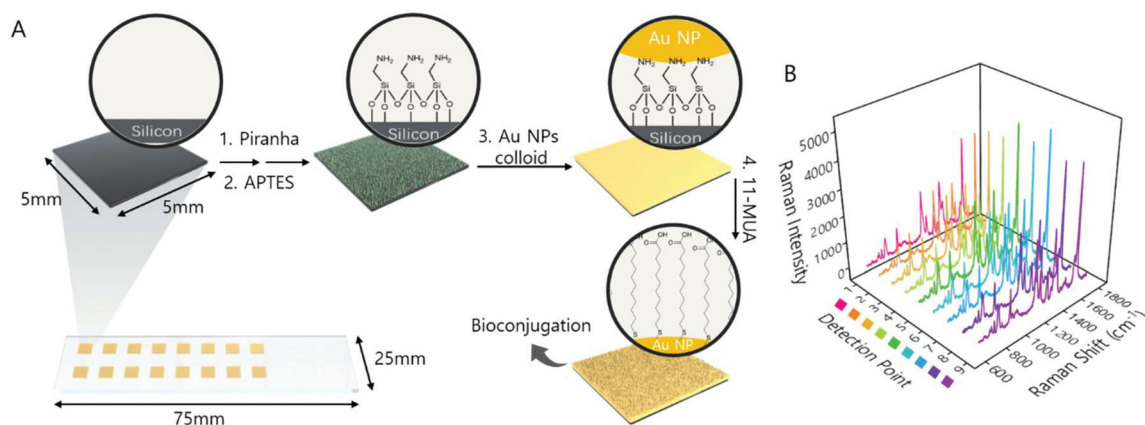
Fig. 5 (A) Fabrication process of gold-patterned chip: (1) silicon wafer washing using piranha solution; (2) functionalization of amino groups with APTES; (3) gold nanoparticles coating on the functionalized silicon wafer; (4) carboxyl group modification on the gold surface. Self-assembly of 11-MUA on the surface of the nanoparticles-embedded gold substrate. (B) Raman spectra of MGITC measured for 9 spots randomly chosen from 2D substrate.

Table 1 Recovery (%) and CV(%) of cTnI and CK-MB for SERS-based assays

Sample type		Endogenous level (ng mL^{-1})	Sample added (ng mL^{-1})	Value obtained (ng mL^{-1})	Recovery^a (%)	CV (%)
No. 1	CK-MB	0.32	10	12.53	112.1	15.1
	cTnI	0.11	10	11.84	98.6	14.7
No. 2	CK-MB	1.55	10	12.87	113.2	13.9
	cTnI	0.12	10	9.85	97.3	10.5

^{a} $\mathrm{Recovery}(\%) = \dfrac{\text{obtained value–endogenous level}}{\text{cTnI/CK-MB added}} \times 100$.

Assessment of SERS-based immunoassay

Fig. 6A and C show the SERS spectra of sandwich immuno-complexes for various concentrations of cTnI and CK-MB ranging from 0 to 100 ng mL^{-1}. Here, different concentrations
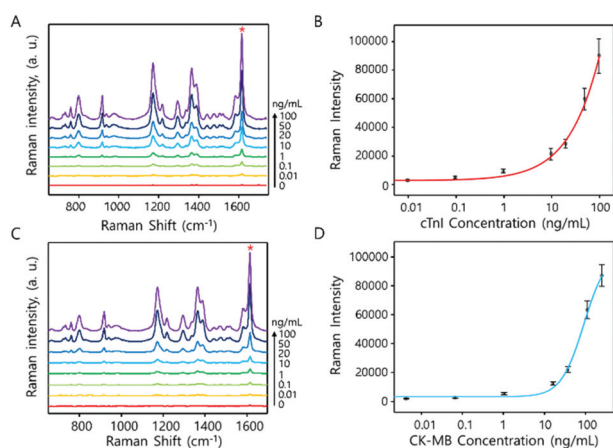
Fig. 6 SERS spectra for increasing concentrations of (A) cTnI and (C) CK-MB. Corresponding calibration curves of the SERS signal intensity at 1615 cm^{-1} as a function of the logarithm of the concentrations of (B) cTnI and (D) CK-MB.

of cTnI and CK-MB were spiked into PBS solution. The SERS intensity of MGITC at 1615 cm^{-1} was utilized for the quantitative evaluation of both target antigens. In the absence of cTnI and CK-MB, no significant SERS signal was observed, indicating that the washing process removed almost all the unreacted SERS probes. Upon the increase of antigens, SERS signals were significantly increased with increasing concentration of both biomarkers. The corresponding calibration curves are shown in Fig. 6B and D. The error bars in the figures indicate the standard deviation of five measurements. Here, a four-parameter logistic fitting model was used to obtain the fitting curves as shown in Fig. S4.† Importantly, the limits of detection (LODs) for the SERS-based immunoassay, estimated as three standard deviations from the background, were 8.9 pg mL^{-1} for cTnI and 9.7 pg mL^{-1} for CK-MB. These results demonstrate that SERS-based sandwich immunoassay utilizing the new SERS probes and the gold-patterned chip has great potential for highly sensitive detection of AMI biomarkers.

Evaluation of SERS-based immunoassay for clinical samples

To assess the clinical applicability of the proposed SERS-based immunoassay method, we performed SERS-based immunoassays on the clinical serum samples. A total of 5 clinical serum samples were collected from the patients with AMI at

Hainan Medical University Hospital. This clinical study was approved by the Institutional Review Board (IRB) at the hospital. Consent documents were also obtained from all patients included in this study. All serum samples were stored at −80 °C until use. Then, the concentrations of cTnI and CK-MB for each of the 5 clinical serum samples were determined using the proposed SERS-based immunoassay. Each clinical sample had been previously detected using a commercially available chemiluminescence assay system installed at Hainan Medical University Hospital. Finally, the SERS-based assay results were compared with those determined by the chemiluminescence assay protocol. As shown in Table S1,† the concentrations of cTnI and CK-MB measured from the SERS-based assay were consistent with those measured from the chemiluminescence system within the clinically acceptable range. Their % coefficient variations (CVs) are also acceptable ranges. Therefore, it could be concluded that our SERS-based assay technique for the detection of dual AMI markers had strong potential as an innovative tool for the *in vitro* screening of AMI.

Conclusion

In the present study, we developed a new SERS-based sandwich immunoassay technique for ultrasensitive detection of AMI biomarkers, using a new SERS nanoprobe (Au@Ag core–shell nanoparticles with double-layered MGITC as Raman reporter molecule) and a gold patterned chip. In the fabrication of gold-patterned chip, home-made gold nanoparticles were immobilized on the surface of amino groups-functionalized silicon wafers to obtain AuNP-coated silicon units. These silicon units were then assembled to fabricate a gold-patterned chip. In addition, Au@Ag core–shell nanoparticles with double-layers of MGITC on the gold core and silver shell were used to construct a kind of new SERS nanoprobes. The thickness of the silver shell was carefully controlled to maximize SERS signal intensity. FDTD simulation was applied to calculate the electromagnetic contribution between Au@Ag nanoparticles, which helps to assess the effect of silver shell on the SERS signal. Finally, the rabbit polyclonal antibodies of cTnI and CK-MB were conjugated on the surface of Au@Ag core–shell NPs and were used for ultrasensitive duplex detection of two biomarkers. The LODs of cTnI and CK-MB determined by this SERS assay protocol could reach 8.9 pg mL^{-1} and 9.7 pg mL^{-1}, respectively, which would be approximately two or three orders of magnitude more sensitive than existing immunoassay techniques based on fluorescence or ELISA. Thus, the SERS-based assay proposed in this study has considerable potential as an effective tool for the early diagnosis of AMI.

Conflicts of interest

There are no conflicts to declare.

Notes and references

1 G. W. Reed, J. E. Rossi and C. P. Cannon, *Lancet*, 2017, **389**, 197–210.
2 F. S. Apple, Y. Sandoval, A. S. Jaffe, J. Ordonez-Llanos and I. T. F. Clinical, *Clin. Chem.*, 2017, **63**, 73–81.
3 R. Twerenbold, A. Jaffe, T. Reichlin, M. Reiter and C. Mueller, *Eur. Heart J.*, 2012, **33**, 579–586.
4 Z. Zhelev, C. Hyde, E. Youngman, M. Rogers, S. Fleming, T. Slade, H. Coelho, T. Jones-Hughes and V. Nikolaou, *Br. Med. J.*, 2015, **350**, 14.
5 R. Navickas, D. Gal, A. Laucevicius, A. Taparauskaite, M. Zdanyte and P. Holvoet, *Cardiovasc. Res.*, 2016, **111**, 322–337.
6 R. P. Tiwari, A. Jain, Z. Khan, V. Kohli, R. N. Bharmal, S. Kartikeyan and P. S. Bisen, *Mol. Diagn. Ther.*, 2012, **16**, 371–381.
7 A. H. B. Wu and R. H. Christenson, *Clin. Biochem.*, 2013, **46**, 969–978.
8 M. Hasanzadeh, N. Shadjou, M. Eskandani, M. de la Guardia and E. Omidinia, *TrAC, Trends Anal. Chem.*, 2013, **49**, 20–30.
9 C. T. Chin, T. Y. Wang, S. Li, S. D. Wiviott, J. A. deLemos, M. C. Kontos, E. D. Peterson and M. T. Roe, *Clin. Cardiol.*, 2012, **35**, 424–429.
10 T. Reichlin, C. Schindler, B. Drexler, R. Twerenbold, M. Reiter, C. Zellweger, B. Moehring, R. Ziller, R. Hoeller, M. R. Gimenez, P. Haaf, M. Potocki, K. Wildi, C. Balmelli, M. Freese, C. Stelzig, H. Freidank, S. Osswald and C. Mueller, *Arch. Intern. Med.*, 2012, **172**, 1211–1218.
11 S. K. Tuteja, M. Kukkar, C. Suri, A. Paul and A. Deep, *Biosens. Bioelectron.*, 2015, **66**, 129–135.
12 W. Y. Lim, T. M. Thevarajah, B. T. Goh and S. M. Khor, *Biosens. Bioelectron.*, 2019, **128**, 176–185.
13 J. Lee, Y.-S. Choi, Y. Lee, H. J. Lee, J. N. Lee, S. K. Kim, K. Y. Han, E. C. Cho, J. C. Park and S. S. Lee, *Anal. Chem.*, 2011, **83**, 8629–8635.
14 K. Zhao, M. Tang, H. Wang, Z. Zhou, Y. Wu and S. Liu, *Biosens. Bioelectron.*, 2019, **126**, 767–772.
15 Y. Liang, X. Huang, X. Chen, W. Zhang, G. Ping and Y. Xiong, *Sens. Actuators, B*, 2018, **259**, 162–169.
16 J. J. Pestka, J. I. Azcona-Olivera, R. D. Plattner, F. Minervini, M. B. Doko and A. Visconti, *J. Food Prot.*, 1994, **57**, 169–172.
17 S. Ren, Y. Li, Q. Guo, Y. Peng, J. Bai, B. Ning and Z. Gao, *Microchim. Acta*, 2018, **185**, 429.

18 L.-J. Zhao, R.-J. Yu, W. Ma, H.-X. Han, H. Tian, R.-C. Qian and Y.-T. Long, *Theranostics*, 2017, **7**, 876–883.

19 H. Lv, Y. Li, X. Zhang, Z. Gao, C. Zhang, S. Zhang and Y. Dong, *Biosens. Bioelectron.*, 2018, **112**, 1–7.

20 N. Liu, H. Yi, Y. Lin, H. Zheng, X. Zheng, D. Lin and H. Dai, *Microchim. Acta*, 2018, **185**, 277.

21 Q. Wu, S. Li, Y. Sun and J. Wang, *Microchim. Acta*, 2017, **184**, 2395–2402.

22 M. Fathil, M. M. Arshad, S. C. Gopinath, U. Hashim, R. Adzhri, R. Ayub, A. Ruslinda, M. Nuzaihan, A. Azman and M. Zaki, *Biosens. Bioelectron.*, 2015, **70**, 209–220.

23 Z. Cheng, N. Choi, R. Wang, S. Lee, K. C. Moon, S.-Y. Yoon, L. Chen and J. Choo, *ACS Nano*, 2017, **11**, 4926–4933.

24 S. Laing, K. Gracie and K. Faulds, *Chem. Soc. Rev.*, 2016, **45**, 1901–1918.

25 G. McNay, D. Eustace, W. E. Smith, K. Faulds and D. Graham, *Appl. Spectrosc.*, 2011, **65**, 825–837.

26 S. Lee, H. Chon, S.-Y. Yoon, E. K. Lee, S.-I. Chang, D. W. Lim and J. Choo, *Nanoscale*, 2012, **4**, 124–129.

27 X. Fu, Y. Wang, Y. Liu, H. Liu, L. Fu, J. Wen, J. Li, P. Wei and L. Chen, *Analyst*, 2019, **144**, 1582–1589.

28 X. Fu, L. Chen and J. Choo, *Anal. Chem.*, 2016, **89**, 124–137.

29 Z. Wang, S. Zong, L. Wu, D. Zhu and Y. Cui, *Chem. Rev.*, 2017, **117**, 7910–7963.

30 D. Zhang, L. Huang, B. Liu, H. Ni, L. Sun, E. Su, H. Chen, Z. Gu and X. Zhao, *Biosens. Bioelectron.*, 2018, **106**, 204–211.

31 N. G. Bastús, J. Comenge and V. Puntes, *Langmuir*, 2011, **27**, 11098–11105.

32 X.-M. Qian and S. M. Nie, *Chem. Soc. Rev.*, 2008, **37**, 912–920.